ARTICLE TYPE www. rsc.org/xxxxxx | XXXXXXXX

Production of cold bromine atoms at zero mean velocity by photodissociation†

W. G. Doherty,[a] M. T. Bell,[a] T. P. Softley,[a] A. Rowland,[b] E. Wrede,[b] and D. Carty[b,c]

Received Xth XXXXXXXXXX 20XX, Accepted Xth XXXXXXXXX 20XX
First published on the web Xth XXXXXXXXXX 20XX
DOI: 10.1039/b000000x

The production of a translationally cold (T < 1 K) sample of bromine atoms with estimated densities of up to 10^8 cm^{-3} using photodissociation is presented. A molecular beam of Br_2 seeded in Kr is photodissociated into Br + Br* fragments, and the velocity distribution of the atomic fragments is determined using (2 + 1) REMPI and velocity map ion imaging. By recording images with varying delay times between the dissociation and probe lasers, we investigate the length of time after dissociation for which atoms remain in the laser focus, and determine the velocity spread of those atoms. By careful selection of the photolysis energy, it is found that a fraction of the atoms can be detected for delay times in excess of 100 μs. These are atoms for which the fragment recoil velocity vector is directly opposed and equal in magnitude to the parent beam velocity leading to a resultant lab frame velocity of approximately zero. The FWHM velocity spreads of detected atoms along the beam axis after 100 μs are less than 5 ms^{-1}, corresponding to temperatures in the milliKelvin range, opening the possibility that this technique could be utilized as a slow Br atom source.

1 Introduction

The production of ultracold atoms and Bose-Einstein condensates[1,2] by the combination of laser cooling and evaporative cooling has been one of the most significant developments in late 20th century physics, and ever-more sophisticated techniques for manipulating and exploring the properties of ultracold matter continue to be developed and extended to other systems. The principal requirement for laser cooling is a closed cycle of absorption and emission in a wavelength range that is compatible with the existence of narrow band laser systems in the IR, visible or near-UV regions. It is widely recognized that this methodology is difficult to apply to molecules[3] but there are also numerous atomic species for which the practical requirements are not met. The halogens F, Cl and Br are examples of atoms for which the lowest one-photon transition lies in the vacuum ultraviolet region (at 104731, 74226 and 63436 cm^{-1} respectively equivalent to $\lambda = 95.48$, 134.73 and 157.64 nm). Presently, suitable laser systems are not available in the VUV region for laser cooling. Alternative methods for producing cold atoms, including surface-contact cooling (for H atoms only[4]), Zeeman deceleration[5,6], and buffer gas cooling[7] have been applied to various species and recently the formation of a BEC of metastable helium atoms has been demonstrated using a combination of buffer gas cooling and evaporative cooling[8]. Some of these techniques could in principle be applied to halogen atoms too, but there have been no such studies to date.

The development of alternative methods to complement laser cooling techniques and to broaden the number of ultracold species available is important not only in the context of understanding the dependence of the physics of quantum degeneracy phenomena on the atomic species employed, but also in the context of cold collision experiments. Exploring the regime of low translational temperatures opens up the prospect of investigating the chemistry and physics of collisional processes in which quantum mechanical effects, such as tunneling and quantum reflection, resonance effects, and restricted angular momentum, may come to the forefront. Controlling the outcome of collisional processes may also become an option at cold and ultracold temperatures, as external fields can significantly perturb the collision dynamics[9].

The halogen atoms and other non-metals such as O and C atoms are highly reactive free-radical species which have traditionally played an important role in the development of the field of chemical reaction dynamics[10]. Many simple reactions of these species have low or negligible activation barriers and are therefore well suited for the study of low temperature chemical dynamics[3]. Calculations for the benchmark system $F + H_2 \rightarrow HF + H$ suggest a remarkably large value for the zero-Kelvin limiting rate constant despite the existence of a barrier in the entrance channel of order $E/k_B = 400$ K[11]. In contrast the $F + D_2$ reaction is predicted to have a zero-Kelvin

[a] *Department of Chemistry, University of Oxford, Chemistry Research Laboratory, Oxford, OX1 3TA, United Kingdom.*
[b] *Department of Chemistry, Durham University, South Road, Durham, DH1 3LE, United Kingdom.*
[c] *Department of Physics, Durham University, South Road, Durham, DH1 3LE, United Kingdom.*

This journal is © The Royal Society of Chemistry [year]

rate that is lower by 2 orders of magnitude[12]. The Cl + H_2 reaction is also a benchmark system and has been investigated theoretically at temperatures down to the ultracold collision energy regime. For Cl + HD ($v = 1$) strong collisional resonances are predicted in the reactive cross section at collision energies below 10 meV[13]. Relaxation of the $^2P_{1/2}$ excited states of F, Cl and Br has been studied both theoretically[14] and experimentally at room temperature[15], but not so far at lower temperatures. The reactions of halogen atoms with the diatomic halogen positive ions are exothermic in some cases, and as discussed below (see Section IV) could be ideal systems for low-temperature studies. There are also intriguing possibilities to study the interaction of cold halogen atoms with cold alkali metal atoms which might enable the production of highly polar cold diatomics (*e.g.*, KCl) by photoassociation or Feshbach resonance tuning. In that context, however, it should be noted that the charge transfer reaction of the excited states of the alkali metals (populated in a laser cooling process) with the halogen atoms is exothermic e.g., K^* + Br $\rightarrow$ K^+ + Br^- . The associative ionization process K^* + Br $\rightarrow$ KBr^+ + e^- would also be energetically feasible. These examples illustrate that the development of an energy-tunable beam of atoms of narrow velocity distribution corresponding to the low-temperature regime of order 1 K or below would be a highly desirable experimental tool in this field.

In this paper we report the demonstration of a new approach to the generation of cold halogen atoms, applied here to bromine atoms, based on the photodissociation of molecular precursors in a supersonic beam. In this technique, the parent molecules in the beam (Br_2 in this case) have a narrow initial velocity distribution centred on a well-defined average velocity. When the molecules are photodissociated, the atomic fragments recoil relative to the centre-of-mass (COM) and the resulting fragment velocity in the lab frame v_{Br} is given by the resultant of the COM recoil, u_{Br}, and the COM velocity, v_{Br_2}, vectors (Figure 1). As illustrated in the figure, the resultant velocity of an atom ejected in the forward direction will be greater than the original beam velocity, but the co-fragment simultaneously ejected backwards will have a lower velocity than the parent. Given the finite angular distribution of the fragmentation in the centre of mass frame, the lab frame velocities will be generally be distributed over a range of angles. By tuning the photolysis energy and extracting atoms ejected in narrow angular range, the mean velocity of the extracted atoms can be selected. In the limiting case, if the energetics of the photodissociation (the excess kinetic energy of the fragments) and the direction of recoil are such that the recoil velocity vector is exactly opposed and of equal magnitude to the parent COM vector, then the resultant velocity of the fragment in the lab frame is zero. Such atoms will remain in the laser-molecular beam interaction zone and after a time delay, these 'photostopped' atoms will be isolated from others.

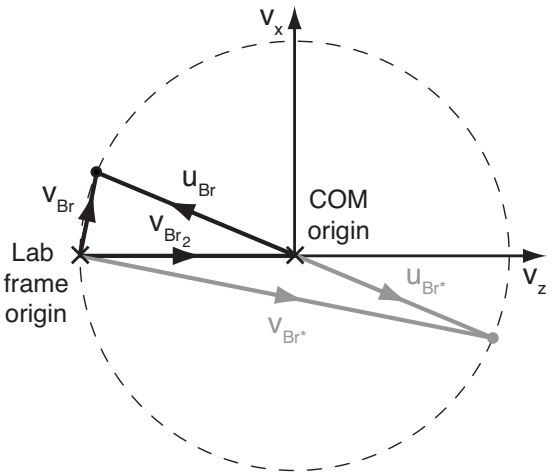

Fig. 1 Newton diagram illustrating how the pair of bromine fragments released almost along the molecular beam axis result in lab-frame velocities which are decelerated (black line, v_{Br}) and accelerated (grey line, v_{Br^*}) relative to the parent molecular beam, v_{Br_2}

This method for producing atoms of low translational energy is closely related to the kinematic cooling of NO molecules[16], in which inelastic collisions, rather than photodissociation recoil, are used to cancel the COM velocity. The present work builds on previous demonstrations of the principles applied to NO_2 photodissociation for production of photostopped NO molecules[17,18].

2 Experimental

2.1 Photolysis scheme and energetics

In the experiments, Br_2 molecules are photodissociated at energies where the principal fragments produced are a combination of one ground state ($Br(^2P_{3/2})$) and one excited state atom ($Br^*(^2P_{1/2})$)[19]. The recoil velocity of the ground state bromine atomic fragments in the COM frame is given by

$$u_{Br} = \sqrt{2\,E_{kin}^{avl} \cdot \frac{m_{Br^*}}{m_{Br} m_{Br_2}}}, \qquad (1)$$

where E_{kin}^{avl} is the kinetic energy available to the fragments, and m_{Br}, m_{Br^*} and m_{Br_2} are the respective masses for Br, Br^* and Br_2. The available kinetic energy is calculated using the energy balance equation,

$$h\nu + E_{int}^{Br_2} - D_0^{Br_2} = E_{kin}^{avl} + E_{int}^{Br} + E_{int}^{Br^*}, \qquad (2)$$

where $h\nu$ is the photon energy, $D_0^{Br_2}$ is the dissociation energy and E_{int} are the internal energies[20] for the respective species ($E_{int}^{Br^*} = 3685.24\ cm^{-1}$ and $E_{int}^{Br} = 0\ cm^{-1}$). By tuning the photon energy $h\nu$, the value of E_{kin}^{avl} can be adjusted to match the

This journal is © The Royal Society of Chemistry [year]

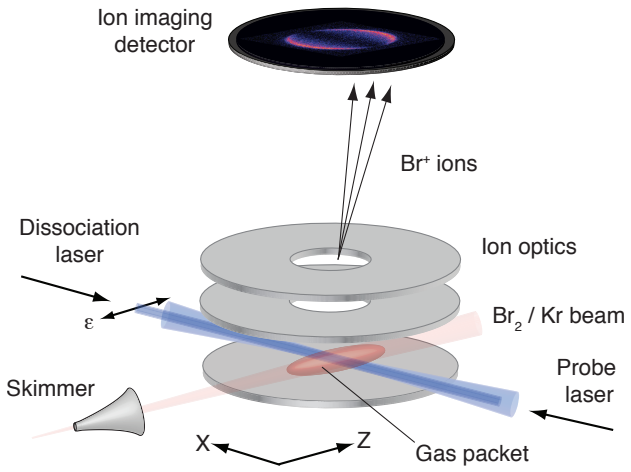

Fig. 2 Schematic of the experimental set-up

fragment velocities to the COM velocity of parent molecules in the molecular beam.

An isotopically pure sample of Br_2 is not used however, implying that there are several different recoil velocities for Br atoms formed from the different parent isotopomers. For the $^{79}Br^{81}Br$ molecule dissociated at 20570 cm^{-1}, the recoil velocities for the ^{79}Br and ^{81}Br atoms are 380.7 and 390.4 ms^{-1}, while for the $^{79}Br^{79}Br$ and $^{81}Br^{81}Br$ molecules, the atomic velocities are 388.2 and 382.9 ms^{-1} respectively, taking account of the slightly different dissociation energies for the isotopomers ($D_0(^{79}Br^{79}Br)$ = 15890 cm^{-1} $D_0(^{79}Br^{81}Br)$ = 15891 cm^{-1} and $D_0(^{81}Br^{81}Br)$ = 15892 cm^{-1} [19]). The spread of velocities has only a very small effect on the kinetic energy distributions reported here but is included in the simulations as discussed below.

The laser polarization vector in the present experiments is parallel to the molecular beam, and therefore the distribution of recoil angles θ relative to the beam axis is given by

$$I(\theta) = \frac{1}{4\pi}\left[1+\beta P_2(\cos\theta)\right], \qquad (3)$$

where $P_2(\cos\theta)$ is the second Legendre polynomial, and β is the recoil anisotropy parameter[21]. The maximum value of β is 2 and this would give rise to a $\cos^2\theta$ distribution of fragment recoil angles, *i.e.*, fragments would be directed principally along the molecular beam axis (both forwards and backwards). For the photodissociation of Br_2 the β value tends to 2 in the photolysis energy range of interest[22], thus the situation is close to optimum.

2.2 Experimental set-up

The experimental set-up (Figure 2) has been described in a previous work[17]. The Br_2 molecular beam is formed by a pulsed (10 Hz repetition rate) supersonic expansion from a 0.5 mm diameter nozzle, using ~10% Br_2 seeded in Kr with a 1 bar backing pressure. The molecular beam (z-axis) passes through a 1 mm diameter skimmer and is intersected at right-angles by two focused laser beams counter-propagating along the x-axis at a distance of 121 mm from the nozzle. The first laser (Nd:YAG 3rd-harmonic pumped dye laser, 3 mJ per pulse) dissociates the Br_2, in the wavelength region of 480-490 nm. In this region, photodissociation results in fragmentation mostly to Br + Br* fragments[19], which is the first electronically excited product channel. A second dissociation channel is available, producing two ground state Br atoms, which have approximately double the COM recoil velocity; the branching ratio to this channel is around 20%. After a variable delay, the probe laser (Nd:YAG 3rd-harmonic pumped dye laser, frequency doubled, 0.15 mJ per pulse) ionizes the bromine atoms remaining in the laser focal region using a (2 + 1) REMPI scheme probing the $^4D_{5/2} \leftarrow {}^2P_{3/2}$ transition at 264.211 nm[20].

A velocity-map ion imaging[23] detection scheme is employed to characterize the dissociation process. The ions are formed in the centre of an electrostatic lens arrangement, which directs the ions towards a microchannel plate (MCP) detector with a phosphorescent screen and CCD camera. The resultant image is a velocity-space map of the ions remaining in the laser focus at the time when the ionizing probe laser pulse arrives; each point on the detector corresponds to a specific velocity in the xz-plane, and each camera pixel corresponds to a velocity spread of 4.0 ms^{-1}, calibrated by taking ion images at a variety of different dissociation wavelengths. Panel A in Figure 3, discussed in more detail below, shows an example of a raw image, observed with a 10 ns delay between the photodissociation and probe lasers. A split ring is observed corresponding to fragments for which the recoil is principally forwards (to the right) or backwards (to the left) with respect to the parent beam direction, in accordance with the expected $\cos^2\theta$ distribution for a β value close to 2. A larger split ring, corresponding to dissociation via the Br + Br channel, can also be observed but is not shown in these images. The zero-velocity point (in the lab frame) was determined by taking an ion image of Br atoms, with a long delay between the firing of the dissociation and probe lasers. A strip was created centered on the zero-velocity point (*e.g.*, Fig. 3, panel E), since only the zero-velocity atoms remained in the excitation volume. The position determined agrees with that of the centre of a thermal distribution of Br_2 molecules leaked into the reaction chamber, detected by non-resonant ionization.

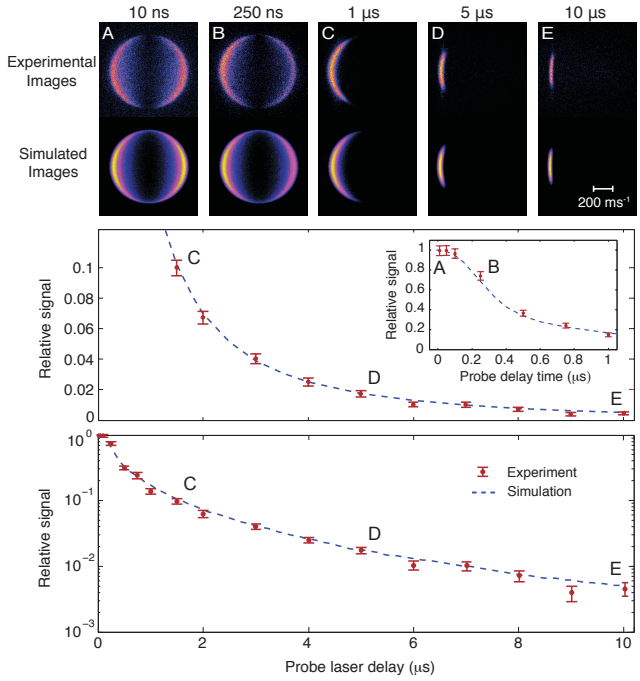

Fig. 3 Top panel: A-E show selected velocity-mapped Br^+ ion images at the indicated delay times for a photolysis wavenumber of 20590 cm^{-1}, with simulated images underneath. Middle panel: Plot of Br^+ ion signal, integrated over the image area shown in the top panel, as a function of the time delay between the dissociation and probe lasers (red) with simulated decay curve (blue). Inset: expanded plot of integrated signal decay at short time delays. Lower panel: As middle, but with the integrated ion signal plotted on a log scale.

The velocity of the molecular beam v_{Br_2} was determined to be 385 ms^{-1}, by taking an ion image of the Br_2 molecules in the beam, seen as a small spot on the detector following (2 + 1) REMPI at 263.012 nm[24]. From this, the FWHM of the velocity distributions are determined to be 45 and 9 ms^{-1} for the z- and x-axis velocities respectively, corresponding to parallel and perpendicular beam temperatures of 15 K and 600 mK. This measurement of the molecular beam velocity allows a determination of the correct photon energy required to produce an equal and opposite fragment recoil velocity. For a beam velocity of 385 ms^{-1}, the required wavenumber is 20590 cm^{-1}.

3 Results

Figure 3 shows the raw ion images obtained as a function of delay time at a photolysis wavenumber of 20590 cm^{-1}, along with the respective simulated images (see below), and a graph of the integrated intensities for each image, normalized to the signal obtained 10 ns after the firing of the photodissociation laser. This small delay is included to eliminate a competing (2 + 1′) REMPI process which contributes a large spike to the Br^+ signal when the probe and photodissociation lasers are overlapped in time. Experimental images (not presented here) were also obtained by ionization of the Br^* atoms at 264.92 nm via the $^4S_{3/2}$ state[20]. In principle an equal number of slow Br^* atoms are formed, as the dissociation process is symmetric about the forward-backward direction; the detection efficiency of Br^* is slightly lower, however, in the current experiments.

The integrated Br^+ signal decays rapidly in the first 400 ns as a result of the bromine atoms that recoil in the forward direction (along the molecular beam axis and hence with $v_{Br} > v_{Br_2}$) leaving the probe laser focus. After this time, the ion images show a single crescent, which arises from the atoms for which at least partial cancellation of the molecular beam velocity has been achieved. For pump-probe delays longer than ∼1 μs, a slower decay in the integrated signal is observed as atoms with predominantly high transverse velocities – those with recoil vectors lying off-axis – are lost from the detection volume. The velocity distributions of the detected Br^+ ions along the x and z directions can be extracted from the images and the FWHM of the distributions are reported in Table 1. Effective translational temperatures in each direction, T_z^{exp} and T_x^{exp} are derived from the velocity distributions of the detected Br^+ ions by assuming the width corresponds to that of a 1D Maxwell-Boltzmann distribution, and values are given in the table.

Simulations of the experiment were performed using a Monte Carlo sampling algorithm, taking into account the full 3D distributions of both the velocities in the parent molecular beam and of the photofragment recoil vectors. Positions

This journal is © The Royal Society of Chemistry [year]

Probe Delay	10 μs	20 μs	50 μs	100 μs
$\Delta v_z^{\rm exp}$ (m s^{-1})	29	21	20	17
$\Delta v_z^{\rm sim}$ (m s^{-1})	28.7	18.6	11.3	10.5
$\Delta v_x^{\rm exp}$ (m s^{-1})	255	219	143	59
$\Delta v_x^{\rm sim}$ (m s^{-1})	263	211	150	75
$T_z^{\rm exp}$ (K)	1.51	0.80	0.73	0.52
$T_x^{\rm exp}$ (K)	112	83.2	35.5	6.0
$\Delta v_z^{\rm Br}$ (m s^{-1})	27	17	7.0	3.9
$T_z^{\rm Br}$ (K)	1.26	0.49	0.09	0.03

Table 1 Velocity spreads (FWHM) and associated temperatures derived from experimental and simulated Br^+ ion velocity distributions along the z- and x-axes (see Fig. 3). The underlying z-velocity spread, $\Delta v_z^{\rm Br}$, and temperature, $T_z^{\rm Br}$, for the neutral Br atoms obtained through simulations is also given. Effective temperatures are defined here assuming a 1D Maxwell-Boltzmann distribution

of the Br_2 molecules were sampled from a uniform random distribution within a cylinder formed by the overlap of the focus of the dissociation laser with the molecular beam, whilst the velocities were obtained from the distribution derived from the experimental VMI measurements of the molecular beam velocity. The velocities of the Br fragments after photolysis were generated by sampling the axially-symmetric distribution given in Eq. 3 over the surface of a sphere, with recoil velocities calculated using Eqs. 1 and 2, assuming a statistical distribution of the Br_2 molecule isotopomers. The expanding bromine atom cloud was assumed to evolve by free flight and the number of atoms remaining in the probe laser volume was recorded after various delay times. For comparison with the experimental images, simulated images were produced by taking 2D histograms of the x- and z-axis velocities of the detectable atoms and calibrated so that the boxes were equivalent in size (in velocity space) to the camera pixels in the experiment. The β parameter was chosen to agree with the experimental value of $+1.8$, as calculated from the images. The experimental measurements of the Br atom velocities are limited by the pixel size in the VMI set-up, the unknown focussing imperfections of the experimental VMI set-up, and by the ion–electron recoil in the REMPI process, equivalent to a velocity gain for the bromine atom of 6.1 ms^{-1}. This recoil is included in the simulations as a velocity kick of constant magnitude with an isotropic angular distribution.

The intensities and shapes of the simulated images were found to be sensitive to the probe-laser ionization volume. This volume was approximated as a cylinder oriented along the probe laser direction, and the radius and length were adjusted to obtain the best agreement with the experimental images; the best match was obtained with a radius 180 μm and length 4 mm. As shown by the dashed line in Figure 3, the simulations accurately predict the probability of creating and detecting bromine atoms in the probe laser volume (the simulated time decay has been normalised to the experimental curve value at 10 ns). Good agreement with the measured velocity distributions along the x and z (right) axes (calculated by integrating the normalised 2D velocity distributions over the v_z and v_x coordinates respectively) is also obtained (Figure 4). At the longest pump-probe times measured (50–100 μs) the experimental z-velocity distributions are limited by the instrumental velocity resolution and thus appear to have a slightly greater spread than predicted by the simulations. The underlying Br atom velocity distributions are expected to be significantly narrower than the Br^+ ion velocity distributions (which are broadened by the photoionization recoil). The velocity-spread and longitudinal temperature values in the final two rows of Table 1 are obtained directly from the simulated Br atom velocity distributions and indicate the z-axis temperature to be lower than 100 mK for times of 50 μs or longer. At such temperatures magnetic trapping of the bromine atoms should be achievable.

An important question is whether there are significant collisional losses of the atoms which are left nearly stationary in the molecular beam as the remainder of the gas pulse passes through. The fit to the decay curve was obtained without assuming any collisional losses. The addition to the simulations of an exponential decay due to collisions could be compensated to some extent (in order to achieve a fit to the experimental decay) by increasing the laser probe volume. However, this would lead to a poor match to the velocity distributions in Figure 3, and therefore it appears that at least in the first 10 μs the effects of collisions are not measurable for the experimental conditions considered here. Collisional heating of the cold atoms is, however, likely to be important for higher intensity beams, as has been observed in the kinematic cooling experiments of Chandler and co-workers[25]. More detailed analysis of these effects requires knowledge of the differential cross section for Br and Kr elastic scattering in order to determine the number of collisions that occur with sufficient transfer of kinetic energy for the Br atoms to be removed from the detection laser focus within the timescales probed during the experiment. This situation is similar to that present in experiments which monitor the loss of a trapped species as a result of elastic collisions[26]: only scattering angles greater than a minimum value lead to loss and so an apparently reduced cross section is observed[27]. Collisional losses may be reduced by using molecular beam pulses shorter than the $\approx$200 μs FWHM pulses employed in the experiments reported here (for example, by using a piezovalve[28])

Whilst an accurate determination of the number density of cold atoms produced is made difficult by the need to determine the absolute detection efficiency in the experiment, an upper

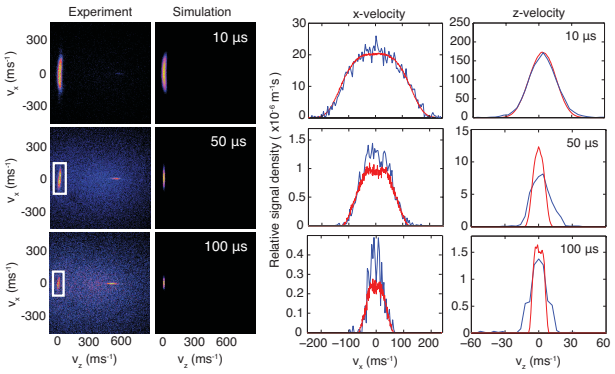

Fig. 4 Experimental ion images with their associated simulated images at increasing delays (left and centre left). The velocity profiles along the x (centre right) and z (right) axes are shown, calculated by integrating the normalised 2D velocity distributions over the v_z and v_x coordinates respectively, with the experimental distributions in blue and simulations in red. See Table 1 for numerical values of the FWHM and associated temperatures of these distributions

limit estimate can be obtained by calculating the density of the bromine molecules seeded in a supersonic expansion of Kr atoms[29,30]. Using the measured Br_2 molecular beam translational temperature of 6 K and assuming the same temperature for the krypton beam, the density of Br_2 molecules at a distance of 121 mm from the 500 μm diameter nozzle is predicted to be of the order of 10^{12}cm^{-3}. The simulations show that the fraction of Br and Br* atoms produced with a kinetic energy less that 1 K (i.e., $\frac{1}{2}mv^2 \leq k_B T$, where $T = 1$ K) is 2.5×10^{-4}. Consequently, when the photodissociation transition is completely saturated, and in the absence of secondary collisions, this fraction of slowly-moving Br atoms is expected to be produced with a density of around 10^8cm^{-3}.

4 Discussion

The technique may be extendable to a range of systems, and indeed the application to NO_2 photodissociation to produce NO molecules with a mean velocity of zero has already been proposed[31] and demonstrated[17,18]. The use of NO photodissociation to produce cold O and N atoms has also been proposed[32], as has the photodissociation of decelerated SO_2 at threshold to produce cold SO and O[33]. With regard to the other halogens, cold chlorine atoms could be similarly produced by photodissociation of BrCl or Cl_2 and both molecules have highly anisotropic dissociation channels[34,35], favouring efficient production of cold atoms. For Cl_2 the appropriate photodissociation wavelength to produce a Cl atom and a Cl* atom with velocities of 560 ms^{-1} (approximate beam speed when seeded in Ar) would be 480 nm, within the chlorine absorption band[36]. For F_2 the technique described here could not be used for producing cold atoms as the absorption cross-section is negligible near the dissociation threshold. The required wavelength corresponding to an F atom velocity of 1800 ms^{-1} (seeding in helium) would be 570 nm, which is well outside the absorption band of F_2. Seeding in heavier gases would move the required wavelength even further outside the absorption band. However the ClF molecule appears to be a promising alternative for production of F atoms. The dissociation energy has been determined to be 21110 cm^{-1}[37] and this energy lies in the middle of the B-X absorption band; indeed predissociation has been observed in this band above the threshold[38].

Applications of cold atoms created using this technique might include the repeated loading of a magnetic trap or storage ring. The current experiment has shown that at the densities employed here, collisional losses are not a major factor. Higher densities may be achievable by moving the photolysis position closer to the nozzle to increase the parent molecule density, but this will also increase the collisional loss rate. Multiple loading of a magnetic trap is also feasible in principle given that the photodissociation could be carried out inside such a trap. Once trapped, it might be possible to attain even lower temperatures, by using, for instance evaporative cooling[8]. The slow moving atoms could also be magnetically guided into a source of cold co-reactants for cold reactive collision experiments, for instance laser- or sympathetically-cooled ions in a radiofrequency trap[39]. By mismatching the fragment recoil and parent molecule velocities, thus creating samples with different mean velocities, it should be possible to create a source of cold atoms with tunable energy, which would be suitable for collisional studies. The atom densities demonstrated in this work are already comparable with neutral molecule densities used in recent ion-molecule experiments in our group[40,41].

Figure 5 shows simulations (using the same parameters as in the simulations of the experimental images in this paper) of the axial velocity distribution of a slow beam of Br atoms created in the entrance of a 5 mm radius, 1 T depth magnetic guide (equivalent to a temperature depth of 1.34 K). The entrance of the guide is positioned so as to collect atoms with a velocity component travelling forwards at an angle of 10 degrees to the molecular beam axis, thus taking atoms out of the molecular beam path. The simulations show that if the photolysis wavelength is varied over the region of absorption for the molecular $B\ ^3\Pi_u(0_u^+)$ state[19] (*ie.* the dissociative channel leading to Br+Br*), then the average kinetic energy can be tuned. In the simulation, the intensities shown reflect the acceptance of the guide due to the kinetic energies of the particles upon mismatching the wavelength, and also include the changing branching ratio to the appropriate dissociation channel with changing photon energy. The simulations show that the original Gaussian profile of the velocity distribution of the

This journal is © The Royal Society of Chemistry [year]

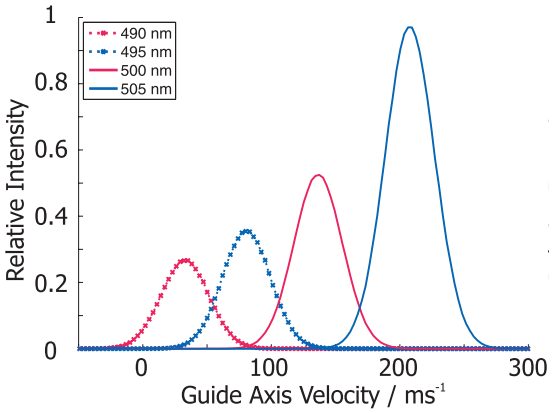

Fig. 5 Simulated velocity distributions of cold bromine atoms along the axis of a magnetic guide, 1 T deep, positioned at an angle of 10 degrees to the molecular beam axis. The parent molecular beam parameters are fixed at their experimentally measured values whilst the dissociation wavelength is varied to control the final velocity of the guided atoms.

molecular beam is essentially maintained in the extracted atom velocity distribution after dissociation, and these atoms can be guided away. The velocity of these atoms is tuneable over a useful range of low velocities (at least 0 to 100 ms^{-1}). The profiles in Figure 5 have FWHM of 45 ms^{-1}. This could be seen as a way of extending the range of energies available to collision experiments involving the halogen atoms, below the minimum threshold energy of atomic molecular beams created by thermal decomposition of the molecular halogens[42], though, clearly with lower number densities. Although slow halogen atoms could also be obtained using the Zeeman deceleration technique[5], the current setup has the advantage of being much more simple to construct.

As discussed in the Introduction, the reactions of halogen atoms, particularly F and Cl, with H_2 have long been benchmark systems for chemical reaction dynamics studies and the development of quantum treatments of chemical reaction rates. However, in the context of current experiments studying cold ion-molecule collisions using laser-cooled and sympathetically cooled ions, an interesting category of reaction for study would be the exothermic reactions of halogen atoms with diatomic halogen ions, e.g., $Br + Cl_2^+ \rightarrow BrCl^+ + Cl$ or $Br + BrCl^+ \rightarrow Br_2^+ + Cl$. The attraction of studying these reactions is that the Cl_2^+ or $BrCl^+$ ions are likely to have long lifetimes with respect to equilibration of rotational populations and if these are formed state-selectively by photoionization then they will be likely to remain in those states on the timescale of the experiments.

5 Conclusions

In summary, this near-threshold photodissociation technique has been successfully applied to the production of bromine atoms with a mean velocity of zero in the laboratory frame and with a velocity distribution characteristic of a temperature <1 K using an appropriately selected photodissociation wavelength; the atoms are observed to remain in the probe volume for more than 100 μs with estimated densities of up to 10^8 cm^{-3}. The technique can be applied with current densities to a range of collisional and spectroscopic experiments and, with further development, offers the potential for applications in ultracold physics.

References

1 M. H. Anderson, J. R. Ensher, M. R. Matthews, C. E. Wieman and E. A. Cornell, *Science*, 1995, **269**, 198–201.
2 J. R. Anglin and W. Ketterle, *Nature*, 2002, **416**, 211–218.
3 M. T. Bell and T. P. Softley, *Mol. Phys.*, 2009, **107**, 99–132.
4 D. G. Fried, T. C. Killian, L. Willman, D. Landhuis, S. C. Moss, D. Kleppner and T. J. Greytak, *Phys. Rev. Lett.*, 1998, **81**, 3811–3814.
5 N. Vanhaecke, U. Meier, M. Andrist, B. H. Meier and F. Merkt, *Phys. Rev. A*, 2007, **75**, 031402.
6 E. Narevicius, A. Libson, C. G. Parthey, I. Chavez, J. Narevicius, U. Even and M. G. Raizen, *Phys. Rev. A*, 2008, **77**, 051401.
7 J. Kim, B. Friedrich, D. P. Katz, D. Patterson, J. D. Weinstein, R. DeCarvalho and J. M. Doyle, *Phys. Rev. Lett.*, 1997, **78**, 3665–3668.
8 S. C. Doret, C. B. Kennedy, W. Ketterle and J. M. Doyle, *Phys. Rev. Lett.*, 2009, **103**, 103005.
9 R. V. Krems, *Phys. Chem. Chem. Phys.*, 2008, **10**, 4079–4092.
10 D. R. Herschbach, *Faraday Discuss.*, 2009, **142**, 9.
11 N. Balakrishnan and A. Dalgarno, *Chem. Phys. Lett.*, 2001, **341**, 652.
12 P. F. Weck and N. Balakrishnan, *Int. Rev. Phys. Chem.*, 2006, **25**, 283–311.
13 N. Balakrishnan, *J. Chem. Phys.*, 2004, **121**, 5563.
14 E. Abrahamsson, G. C. Groenenboom and R. V. Krems, *J. Chem. Phys.*, 2007, **126**, 184303.
15 R. J. Donovan and D. Husain, *Trans. Faraday Soc.*, 1966, **62**, 2987 – 2993.
16 M. S. Elioff, J. J. Valentini and D. W. Chandler, *Science*, 2003, **302**, 1940–1943.
17 A. Trottier, E. Wrede and D. Carty, *Mol. Phys., In Press*, 2011.
18 B. S. Zhao, S. E. Shin, S. T. Park, X. Sun and D. S. Chung, *J. Phys. Soc. Japan*, 2009, **78**, 094302.
19 M. J. Cooper, E. Wrede, A. J. Orr-Ewing and M. N. R. Ashfold, *J. Chem. Soc., Faraday Trans.*, 1998, **94**, 2901–2907.
20 N. A. S. Database, `http://www.nist.gov/pml/data/asd.cfm`.
21 R. N. Zare, *Angular Momentum*, Wiley, New York, 1988.
22 E. Wrede, E. R. Wouters, M. Beckert, R. N. Dixon and M. N. R. Ashfold, *J. Chem. Phys.*, 2002, **116**, 6064.
23 A. T. J. B. Eppink and D. H. Parker, *Rev. Sci. Instr.*, 1997, **68**, 3477–3484.
24 M. Beckert, S. J. Greaves and M. N. R. Ashfold, *Phys. Chem. Chem. Phys.*, 2003, **5**, 308–314.
25 K. E. Strecker and D. W. Chandler, *Phys. Rev. A*, 2008, **78**, 063406.
26 T. V. Tscherbul, Z. Pavlovic, H. R. Sadeghpour, R. Cote and A. Dalgarno, *Phys. Rev. A*, 2010, **82**, 022704.

27 D. E. Fagnan, J. Wang, C. Zhu, P. Djuricanin, B. G. Klappauf, J. L. Booth and K. W. Madison, *Phys. Rev. A*, 2009, **80**, 022712.
28 D. Irimia, D. Dobrikov, R. Kortekaas, H. Voet, D. A. van den Ende, W. A. Groen, and M. H. M. Janssen, *Rev. Sci. Instrum.*, 2009, **80**,.
29 G. Scoles, *Atomic and Molecular Beam Methods*, OUP, New York, 1988.
30 S. DePaul, D. Pullman and B. Friedrich, *J. Phys. Chem.*, 1993, **80**, 2167.
31 S. J. Matthews, S. Willitsch and T. P. Softley, *Phys. Chem. Chem. Phys.*, 2007, **9**, 5656 – 5663.
32 B. Clarson, S. R. Procter, A. L. Goodgame and T. P. Softley, *Mol. Phys.*, 2008, **106**, 1317–1330.
33 S. Jung, E. Tiemann and C. Lisdat, *Phys. Rev. A*, 2006, **74**, 040701.
34 M. Beckert, E. R. Wouters, M. N. R. Ashfold and E. Wrede, *J. Chem. Phys.*, 2003, **119**, 9576–9589.
35 P. C. Samartzis, B. L. G. Bakker, T. P. Rakitzis, D. H. Parker and T. N. Kitsopoulos, *J. Chem. Phys.*, 1999, **110**, 5201–5207.
36 Y. Matsumi, K. Tonokura and M. Kawasaki, *J. Chem. Phys.*, 1992, **97**, 1065–1071.
37 V. A. Alekseev and D. W. Setser, *J. Chem. Phys.*, 1997, **107**, 4771–4782.
38 I. S. McDermid, *J. Chem. Soc., Faraday Trans. 2*, 1981, **77**, 519–530.
39 S. Willitsch, M. T. Bell, A. D. Gingell and T. P. Softley, *Phys. Chem. Chem. Phys.*, 2008, **10**, 7200–7210.
40 M. T. Bell, A. D. Gingell, J. M. Oldham, T. P. Softley and S. Willitsch, *Faraday Discuss.*, 2009, **142**, 73–91.
41 A. D. Gingell, M. T. Bell, J. M. Oldham, T. P. Softley and J. N. Harvey, *J. Chem. Phys.*, 2010, **133**,.
42 J. J. Valentini, M. J. Coggiola and Y. T. Lee, *Rev. Sci. Instr.*, 1977, **48**, 58–63.

This journal is © The Royal Society of Chemistry [year]